June 1996 • NREL/TP-413-21355

Application of CIS to High-Efficiency PV Module Fabrication

Annual Technical Progress Report
1 April 1995 - 31 March 1996

B. Başol, V. Kapur, C. Leidholm,
and A. Halani
International Solar Electric Technology
Inglewood, California

National Renewable Energy Laboratory
1617 Cole Boulevard
Golden, Colorado 80401-3393
A national laboratory of the U.S. Department of Energy
Managed by Midwest Research Institute
for the U.S. Department of Energy
under Contract No. DE-AC36-83CH10093

NREL/TP-413-21355 • UC Category: 1260 • DE96007913

Application of CIS to High-Efficiency PV Module Fabrication

Annual Technical Progress Report 1 April 1995 - 31 March 1996

B. Başol, V. Kapur, C. Leidholm, and A. Halani
International Solar Electric Technology
Inglewood, California

NREL technical monitor: H.S. Ullal

National Renewable Energy Laboratory
1617 Cole Boulevard
Golden, Colorado 80401-3393
A national laboratory of
the U.S. Department of Energy
Managed by Midwest Research Institute
for the U.S. Department of Energy
under Contract No. DE-AC36-83CH10093

Prepared under Subcontract No. ZAF-5-14142-07

June 1996

NOTICE

Available to DOE and DOE contractors from:
Office of Scientific and Technical Information (OSTI)
P.O. Box 62
Oak Ridge, TN 37831
Prices available by calling (423) 576-8401

Available to the public from:
National Technical Information Service (NTIS)
U.S. Department of Commerce
5285 Port Royal Road
Springfield, VA 22161
(703) 487-4650

TABLE OF CONTENTS

LIST OF FIGURES

LIST OF TABLES

1.0 SUMMARY

This is the Phase I Annual Technical Report of the subcontract titled "Application of CIS to High Efficiency PV Module fabrication." The general objectives of the program are the development of a novel, non-vacuum process for CIS film deposition, optimization of the various layers forming the CIS device structure, and fabrication of high efficiency submodules. The specific goals of the project are the development of 11% efficient cells and 8% efficient submodules using a novel, low-cost CIS deposition approach.

During this research period, we investigated the interactions between the soda-lime glass substrate, the Mo contact film and the CIS absorber layer. Excessive Na diffusion through the Mo layer was found to be the reason for excessive interaction between the substrate and the CIS layers obtained by the H_2Se selenization technique. This chemical interaction was found to have influence on the stoichiometric uniformity of the absorbers. A Na diffusion barrier needs to be developed to avoid this problem.

Addition of Ga into the CIS layers by the two-stage selenization technique yielded graded absorber structures with higher Ga content near the Mo/absorber interface. Gallium was later diffused through the absorber film by a high temperature annealing step and large bandgap alloys were obtained. Solar cells with active area efficiencies of close to 12% were fabricated on these CIGS layers. Sulfur addition experiments were also carried out during this period. By controlling the Se and S availability to the precursors during the reaction step of the process, various S profiles were obtained in high bandgap absorber layers. The highest efficiency cell made on S-containing absorbers was about 10% efficient.

A low-cost, non-vacuum technique was successfully developed for CIS film growth. Layers prepared using this novel approach were used for solar cell and submodule fabrication. Solar cells with active area efficiencies around 13% were demonstrated. Submodules with efficiencies above 8% were also fabricated. These results represent the best PV devices ever produced on CIS layers obtained by a non-vacuum technique.

2.0 INTRODUCTION

This is the Phase I Annual Technical Report of a subcontract titled "Application of CIS to High Efficiency PV Module Fabrication". The objective of this program is to develop understanding and solutions for certain issues related to cost-effective production of CIS-based PV modules. The most important task is the development and demonstration of a novel, low-cost method for CIS film growth that does not employ expensive vacuum processing. Another task involves study of Ga and/or S addition into the CIS absorber layers for bandgap tailoring.

Recent advances made in CIS and related compound solar cell fabrication processes have clearly shown that these materials and device structures can yield power conversion efficiencies greater than 15%. Thin film CIS solar cells fabricated at ISET employing the two-stage selenization process have achieved conversion efficiencies of around 13%. ISET's two-stage process for CIS thin film growth involves selenization of metallic Cu-In precursors. In this approach the Mo coated glass substrate is first coated with a thin layer of Te. This step is then followed by the sequential deposition of In and Cu layers. The resulting films are highly alloyed Cu-In precursors that can be repeatably processed into good quality CIS layers. For CIGS absorber formation, Ga can be added into the precursor layer. The details of these processes and the results obtained were described in our 1995 Final Report [1] and will not be repeated here. The following sections of this report will provide information about three major areas of research carried out during the last 12-month period, i.e., investigation of CIS-Mo-substrate interactions, studies on large bandgap absorber layers and development of a novel, non-vacuum CIS deposition technique.

The specific goals of this 12-month program as listed in the "Statement of Work" and the "Schedule of Deliverables" are : The development of 11% efficient cells of 1 cm^2 area and 8% efficient submodules of 4"x4" area using a novel, low-cost, non-vacuum CIS growth technique.

3.0 TECHNICAL DISCUSSION

Details of ISET's baseline selenization technique and the device fabrication steps have been previously described [1]. In summary, these baseline processes involved vacuum deposited metallic precursors and vapor phase selenization. Cu-In precursors of various stoichiometries were deposited onto Mo-coated soda-lime glass substrates at room temperature using the evaporation and sputtering methods. Gallium addition into the absorber layers was achieved by adding a thin layer of Ga into the Cu-In precursor stack. Selenization of the precursors was carried out in a reactor kept at a temperature of about 400 °C. The reactive atmosphere in the selenization chamber contained a mixture of H_2Se gas and Ar. For device fabrication, CIS films were coated with a thin (600-2000 Å) CdS layer using the solution growth technique. This step was then followed by the deposition of a conductive ZnO window layer using the MOCVD method.

It should be noted that the above described CIS film growth technique was only used for the tasks involving Ga/S addition to the absorbers and for the task that was designed to study the substrate/film interactions. Tasks involving the development of a novel CIS growth approach naturally did not have any vacuum deposition step. In these tasks, films were grown through a new non-vacuum technique. Device fabrication steps, however, were common to CIS absorbers obtained by both vacuum and non-vacuum approaches.

3.1 CIS-Mo-Substrate Interactions

Although, glass is commonly distinguished by its high chemical resistance at low temperatures, its reactivity may actually be extensive at temperatures and chemical environments employed in CIS film growth. The typical composition of a soda-lime glass sheet in weight percentages is 70% SiO_2, 15% Na_2O, and the balance, the oxides of Ca, Al, Mg, Ba and K [2]. The Na-O network in soda-lime glass is known to be reactive and we had previously studied the extensive reactions that are possible between the Na in the glass substrate and the selenization environment.

Mo is the contact layer that stands between the selenization environment and the soda-lime glass substrate. If no prior processing is done on the surface of the soda-lime glass substrate, Mo can act as the barrier or the conduit to the diffusion of Na from the glass substrate into the growing CIS layer. In our previous work we had shown that the diffusion of Na through a Mo contact layer depended on various factors such as the structure and chemical content of the Mo film. During this period we have carried out further experiments to shed light on this very important topic.

Mo films were grown in a sputtering system with vertical geometry. The soda-lime glass substrates were passed in front of a DC magnetron cathode at a controlled speed to deposit 1-3 μm thick layers. Mo/glass samples as well as Mo/glass/Cu-In structures were

selenized in a H_2Se atmosphere at around 400 °C for about 30 minutes. Auger depth profiling was used to determine the distribution of the reaction products through the selenized layers. XPS measurements were also employed to investigate the chemical nature of these products. Some of these experiments were carried out as part of the teaming effort coordinated by NREL.

A set of six samples were analyzed by AES measurements. This set contained the following samples:

Sample Mo134 ("good"Mo on soda lime glass substrate).
Sample Mo317 ("bad" Mo on soda-lime glass substrate).
Sample Mo134 selenized.
Sample Mo317 selenized.
Sample Mo134 with a thin CIS layer deposited on it (CIS/Mo/glass structure).
Sample Mo317 with a thin CIS layer deposited on it (CIS/Mo/glass structure).

The Auger depth profiles of Fig. 1a and 1b were taken from the two as-deposited Mo samples. The profiles obtained from these Mo layers after the selenization step are given in Fig. 1c and 1d. The thickness of Mo134 was about 1.5 μm, whereas, Mo317 was 0.7 μm thick.

Auger profiles of Fig. 1 show fluctuations in the intensities of the Mo signals through the two films studied. Every decrease in Mo signal coincides with an increase in the level of the O signal. These fluctuations in the Mo signal are due to the fact that the Mo films of this experiment were deposited in the form of multiple layers (multiple passes in front of the Mo target). Apparently every time the film went through the plasma region of the target and the deposition was terminated until the next pass, some oxidation took place on the surface of the deposited film giving rise to the high oxygen regions observed in the Auger data. The Mo layer of Fig.1a had six such layers. The Mo film of Fig. 1b was prepared in only two passes in front of the sputtering target as confirmed by the Auger measurement. One interesting observation from the data of Fig. 1 is the difference between the two Mo films in terms of their oxygen content. The background oxygen content of the film of Fig. 1a is about 10%, whereas, this value is less than 2% for the film of Fig. 1b. Surface survey of these two as-deposited Mo layers indicated that no appreciable Na diffusion took place through the layers during the Mo deposition step since no Na signal was observed on their surface. After selenizing the above mentioned Mo samples, however, a large Na signal appeared along with a strong O signal on the surface of the "bad" Mo (Mo317). There was still no Na on the surface of the "good" Mo sample. The above analysis confirmed that our "good" Mo samples were better barriers to Na diffusion. The question is whether this property of the Mo could be related to its oxygen content. It is quite possible that formation of Mo bronzes along the oxygen containing grain boundaries may chemically trap the Na and slow down its diffusion into the CIS layer. Of course, one other possible explanation for the difference in the barrier nature of the two Mo layers could be the difference in their thicknesses. The "good" Mo of this experiment was much thicker than the "bad" Mo.

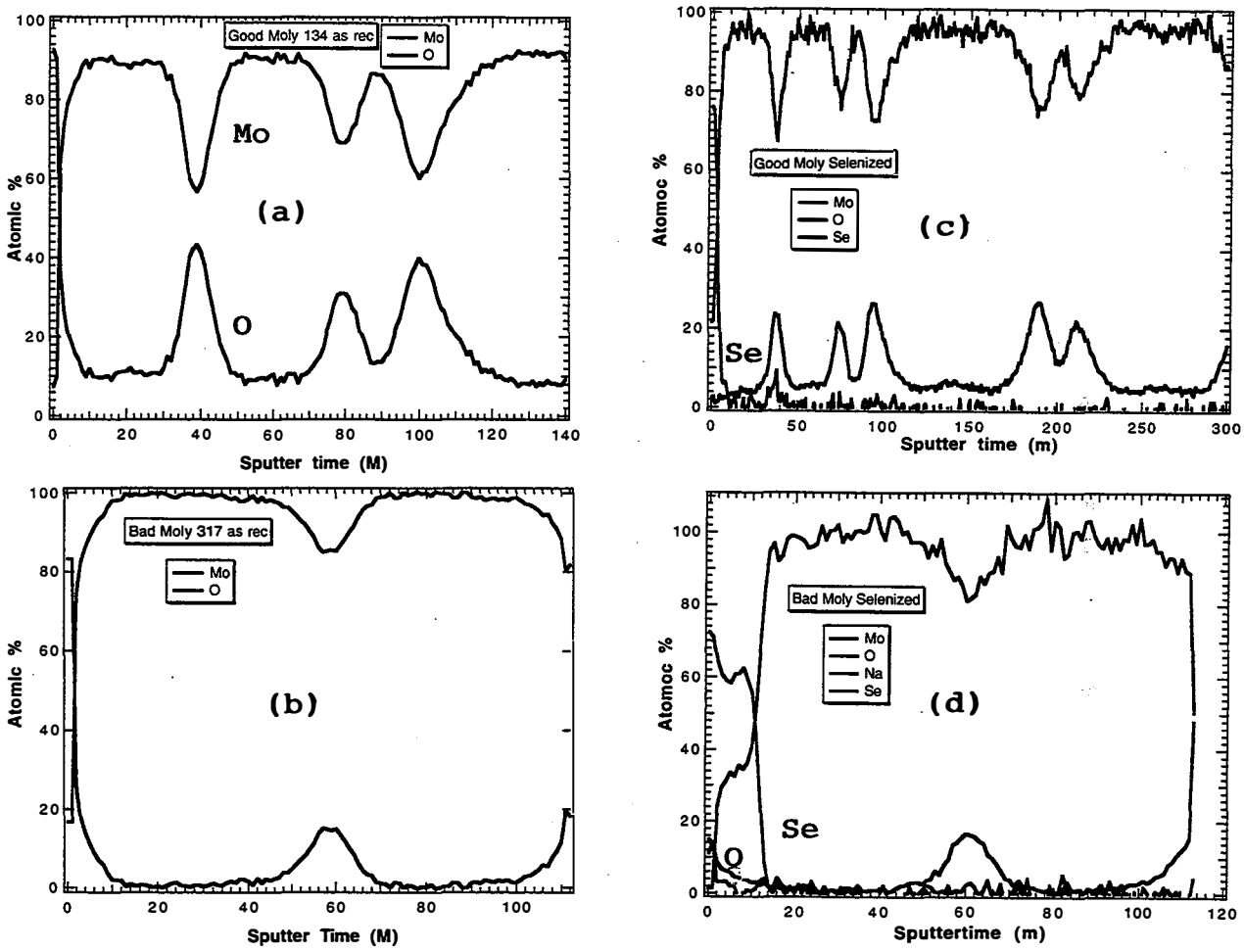

Fig. 1 Auger depth profiles of Mo134 ("good" Mo) and Mo317 ("bad" Mo) samples (a), (b) before, and (c) (d) after selenization.

However, we have carried out experiments on Mo layers that were deposited under the same conditions as Mo317, only thicker. The observations after selenization did not change. In other words, "bad" Mo was a bad barrier to Na diffusion irrespective of its thickness.

The Auger depth profiles of Fig. 2 were taken from the two CIS/Mo/glass structures listed before as the samples with thin CIS layers. In these samples the Cu-In precursors were intentionally made thin as to yield CIS layers of about 0.5 μm thickness after the selenization step. The goal here was to amplify any possible effect of the glass/Mo substrate on the growth of the thin CIS film. The Mo layers used in this experiment were labeled as "good" and "bad", again indicating Mo134 and Mo317, respectively. There are several observations one can make from the data of Fig. 2.

First of all, it is clear that the CIS layer deposited on the "good" Mo substrate behaves normally with Cu and In profiles closely following each other suggesting a Cu/In stoichiometric ratio close to 1.00. The Auger depth profile of Fig. 2b, on the other hand, shows a highly non-uniform CIS layer with a high In content near the surface and a rising Cu signal near the CIS/Mo interface. The large difference between the atomic percentages suggested by the Auger data actually points out that the film is not single phase CIS. There is also a prominent oxygen peak near the film/Mo interface as was the case in Fig. 1d. In our past studies we had only investigated the reactions between the glass/Mo structures and the H_2Se selenization atmosphere. The data of Fig. 2 suggests that the CIS layer itself may also be reacting with the underlying substrate. In fact, according to the data of Fig. 2 the local stoichiometry of the CIS film can be influenced by the reactivity of the underlying Mo layer. There may be more than one explanation for the increased Cu content near the CIS/Mo interface of the sample of Fig. 2b. Formation of a Mo-Se-Na-O-Cu compound at this interface is a possibility. One other possibility is the formation of Mo-Se compounds which are known to be layered and which can act as a sink for Cu diffusion.

In addition to the investigation described above we have carried out other experiments where solar cell performance on "good" and "bad" Mo substrates were compared. SIMS analysis was also done on the CIS layers deposited on the two types of Mo layers. All the experiments pointed to the fact that Na diffusion through "bad" Mo substrates was excessive and solar cells fabricated on such layers suffered from poor fill factor and thus lower efficiency. Clearly there is a need to develop a barrier layer on the soda-lime glass substrates for Na diffusion. With such an approach there will also be a need to controllably introduce Na in the CIS film during the growth process. ISET's new non-vacuum CIS growth technique is well suited for such an approach and this task will be carried out during the Phase II program.

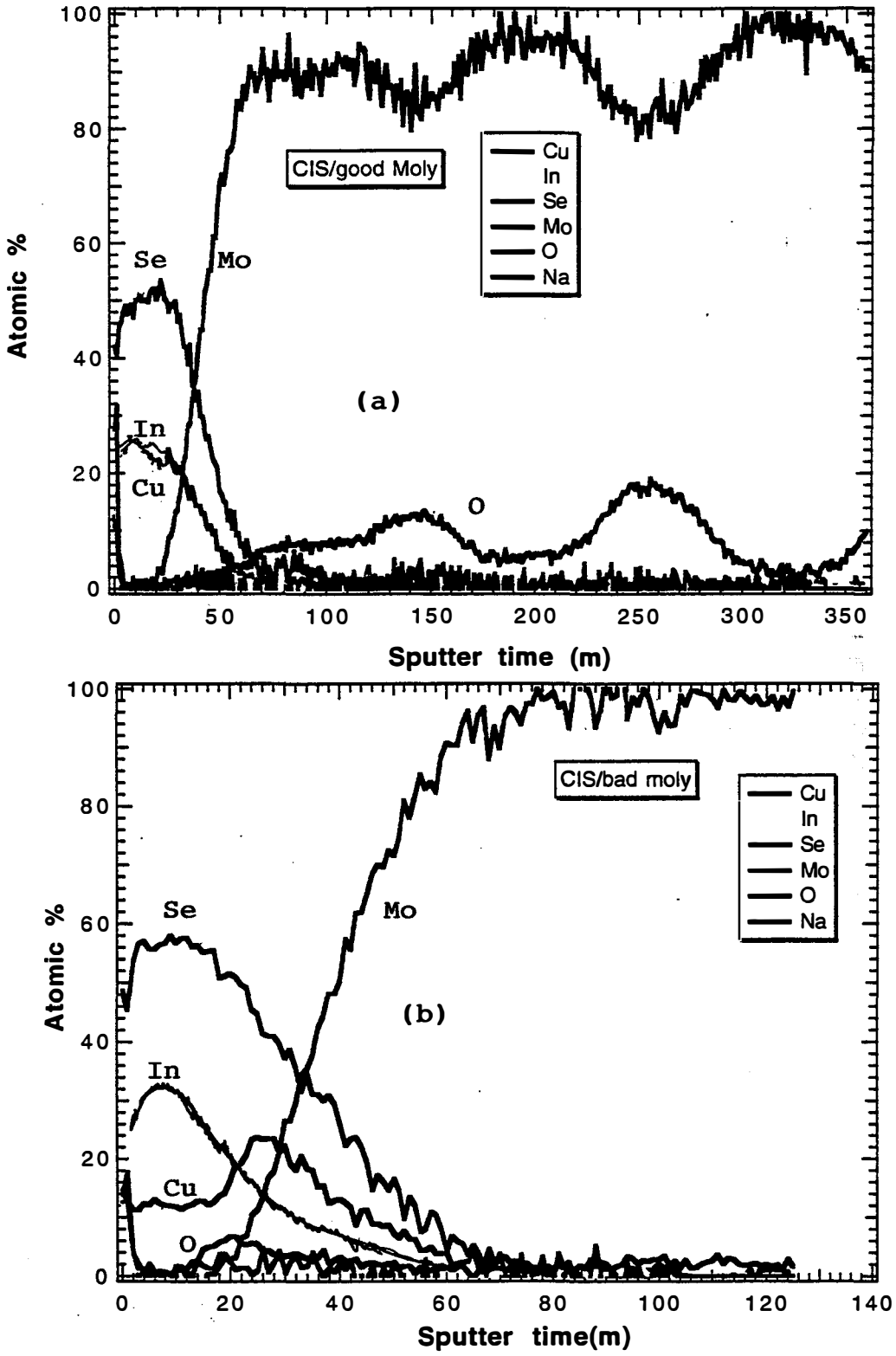

Fig. 2 Auger depth profiles of a) CIS/Mo134 and CIS/Mo317 samples.

3.2 Studies on Large Bandgap Absorber Layers

3.2.1 Films containing Ga

To date, the highest efficiency devices have been fabricated on CIGS films with graded Ga distribution obtained by a multi-source evaporation technique [3]. As for the selenization approaches, Kushiya et al. prepared CIGS layers with uniform Ga and In distributions by the selenization of co-evaporated Cu+In+Ga+Se precursor layers in a vacuum system and demonstrated a 14.9% efficient device on a film with a Ga/(Ga+In) ratio of 0.40 [4]. Unlike the results of Kushiya et al. on films grown by the selenization of co-evaporated Cu+In+Ga+Se precursors, co-evaporated Cu+In+Ga metallic precursor layers always yielded absorbers with graded Ga concentrations when selenized in a vacuum system under Se vapor [5]. In such films, Ga-rich phase(s) segregated toward the back of the absorber layer, leaving an In-rich surface. Films grown by the selenization of Cu+In+Ga metallic precursors in H_2Se-containing atmospheres showed very similar behavior [6,7]. The reasons for this behavior are not well understood. However, it is possible that the In-Se reactions which are more energetically favorable at low temperatures form the driving force for In to selectively diffuse to the surface region to react with the selenizing atmosphere as the temperature of the substrate is raised.

Segregation of Ga-rich and In-rich phases by depth, in absorber layers obtained by the selenization of metallic precursors, does not allow the growth of CIGS films with uniform composition. A Ga-rich region deep in the absorber layer can benefit device performance because this high-bandgap area can induce an electric field in the bulk of the absorber and help minority carrier collection from deep in the device. However, segregation of the Ga-rich and In-rich phases in a manner that leaves a small-bandgap CIS surface would limit the open-circuit voltage values of devices fabricated on such absorbers. In a recent publication, the IEC group at the University of Delaware demonstrated that films obtained by the selenization of metallic precursors displayed total segregation of CIS and CGS phases when further annealed in an H_2Se atmosphere at high temperatures. They also described a new process consisting of a post-selenization annealing step in a Se-free atmosphere, which was found to be essential to initiate the diffusion of Ga and formation of the quaternary CIGS phase [6]. In this work, we employed the post-selenization step of reference 6 to grow CIGS absorber layers with an overall Ga/(Ga+In) ratio of 0.55-0.75, characterized these layers in terms of their structural and compositional properties, and evaluated their application to high-efficiency solar cell fabrication.

Soda-lime glass was used as the substrate in this work. Molybdenum layers were sputter deposited on the soda-lime glass substrates using a D.C. magnetron system. CIGS absorber films were formed on the Mo/glass sheets by the two-stage selenization technique employing precursors containing In, Cu and Ga. Thicknesses of the In, Cu, and Ga layers were adjusted to obtain films with various compositions and an overall stoichiometric ratio of about Cu/(In+Ga)=0.9. For the precursor of samples 1789-425 and

1789-575, the overall Ga/(Ga+In) ratio was 0.55 and the thicknesses of the evaporated In, Cu, and Ga layers as monitored by a crystal oscillator head were 2223 Å, 2000 Å, and 2027 Å, respectively. The Ga/(In+Ga) ratio for the precursor of samples 1791-425 and 1791-575, on the other hand, was 0.75, with corresponding elemental film thicknesses of 1228 Å, 2000 Å and 2765 Å.

Selenization was carried out for all precursors at 425 °C . A portion of each film was then additionally annealed at 575°C in a N_2 atmosphere. Resulting selenide films were nominally 2.0 μm thick, and they were analyzed by scanning electron microscopy (SEM), X-ray diffraction (XRD), and Auger depth profiling. Auger analysis was carried out by a Physical Electronics 670 microprobe using a 5 kV electron beam. The samples were depth profiled using a 3 kV argon ion sputtering beam. A reference CIGS sample with uniform Ga distribution deposited at NREL by the co-evaporation technique was used to calibrate the Auger sensitivity factors for Cu, In, Ga, and Se based on electron microprobe measurements. Devices were fabricated by depositing a thin layer of CdS on the CIGS layers by the solution growth technique. Conductive ZnO window layers were deposited by the metal-organic chemical vapor deposition (MOCVD) approach using diethylzinc (DEZ) and water vapor as the reactants and boron as the dopant. Table I contains the relevant information about processing all the samples.

A. Device Measurements

Figure 3 shows the illuminated J-V characteristics of solar cells fabricated on three of the absorber layers identified in Table I. The devices fabricated on sample 1791-425 were extremely leaky, and since they did not display a photovoltaic response, they were not included in Fig. 3.

The J-V characteristics of Fig. 3 indicate an open-circuit voltage (V_{oc}) value of 740 mV for sample 1791-575 and 625 mV for sample 1789-575. The V_{oc} for sample 1789-425, on the other hand, is only 400 mV despite the fact that this film contained 55% Ga. The absolute QE curves given in Fig. 4 were normalized using the short-circuit current values of the three devices. The losses due to various factors such as grid coverage and contact probe shadowing are shown in this figure. Reflection, ZnO absorption and CdS absorption measurements were made on a set of reference samples of CdS and ZnO on glass. The QE curves demonstrate that the effective bandgaps of the three absorbers varied from 1.05 eV for sample 1789-425 to 1.36 eV for sample 1791-575. The solar cell output parameters derived from Fig. 3 as well as the E_g values are summarized in Table II. E_g values were deduced from the shift of the long wavelength QE of the cells compared with a pure CIS device with the bandgap value of 1.00 eV. Long wavelength QE of the CIS cell is also shown in Fig. 4 for reference. The estimated uncertainty in the E_g values is 30 mV. The following observations can be made from the data of Table II:

(i) The bandgap value of sample 1789-425 deduced from its QE curve was much less than the 1.4 eV expected from a uniform CIGS layer with 55% Ga. The observed

Sample No.	Overall Composition of the Precursor		CIGS Formation Steps	
	Cu/(In+Ga)	Ga/(Ga+In)	Selenization	Annealing
1789-425	0.9	0.55	425°C, 30 min.	
1789-575	0.9	0.55	425°C, 30 min.	575°C, 60 min
1791-425	0.9	0.75	425°C, 30 min	
1791-575	0.9	0.75	425°C, 30 min.	575°C, 60 min.

Table I Information on the CIGS films grown for this study.

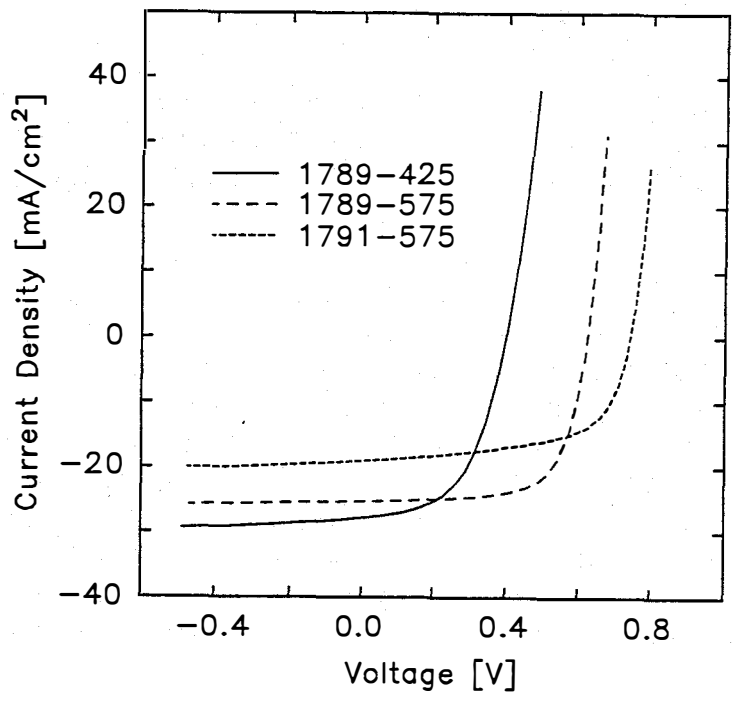

Fig. 3 Illuminated J-V characteristics of three solar cells fabricated on CIGS films. Sample numbers are shown in the insert. Data was taken under AM1.5 illumination. Active area of cells was 0.083 cm^2.

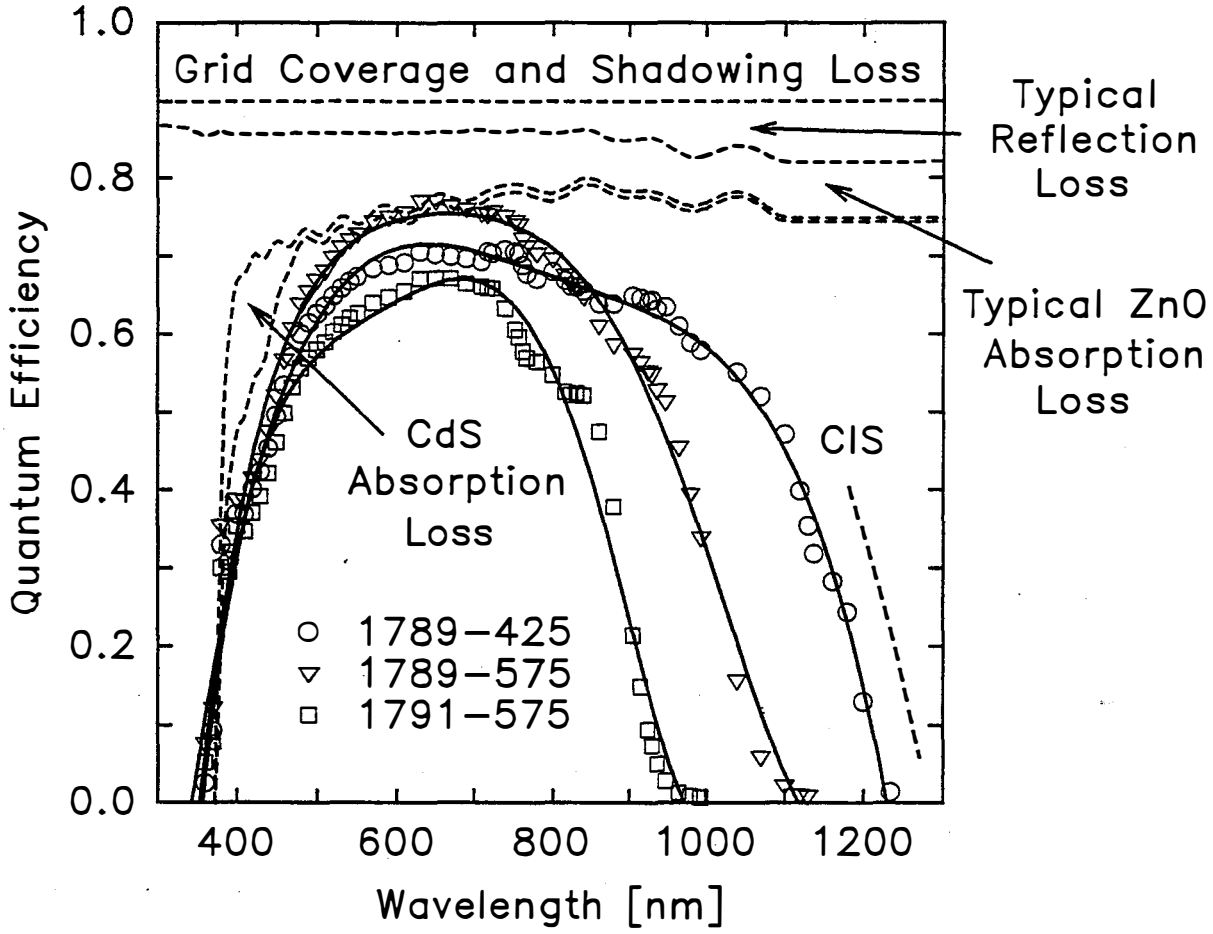

Fig. 4 Absolute quantum efficiencies of the cells of Fig. 3.

Sample No.	η (active area)	FF	V_{oc} (mV)	J_{sc} (mA/cm^2)	E_g (eV)
1789-425	6.4	0.54	400	30	1.05
1789-575	11.7	0.69	625	27.3	1.19
1791-575	9.4	0.615	740	20.6	1.36

Table II Solar cell parameters and bandgap values derived from the data of Fig. 3 and Fig. 4. Active area of the devices was 0.083 cm^2.

value of E_g= 1.05 eV and correspondingly modest V_{oc} value of 400 mV, suggest the presence of a CIGS composition with only about 7% Ga in the absorber layer. Furthermore, the solar cell fabricated on this absorber is relatively poor with a low fill-factor value.

(ii) High-temperature annealing of sample 1789-425 increased the effective bandgap of this absorber to 1.19 eV and V_{oc} to 625 mV, indicating increased Ga activity. However, this bandgap is still lower than the 1.4 eV expected from a uniform CIGS layer with 55% Ga. The measured bandgap value of 1.19 eV indicates the presence of a CIGS phase in the absorber with about 28% Ga.

(iii) The QE data obtained from the cell fabricated on the annealed sample with overall Ga content of 75% yielded a bandgap value of 1.36 eV and the device had a V_{oc} of 740 mV, which corresponds to a CIGS phase with about 50% Ga.

The open-circuit voltages of the three devices of Fig. 3 were measured in the temperature range of 270-350 K. Extrapolation of V_{oc} to T=0 K gave an estimate of E_g , assuming it changes little over the temperature range used. The zero-temperature intercepts were 1.08 eV, 1.25 eV, and 1.34 eV for samples 1789-425, 1789-575, and 1791-575, respectively. These values are in reasonable agreement with the values obtained from QE data and listed in Table II.

Figure 5 shows the cross-sectional EBIC line scans of two devices superimposed over their scanning electron images. The various layers forming the device structure are labeled on this figure. The CIGS layers are dense and are composed of grains as large as 1-2 μm. The grain size does not seem to be a function of the high-temperature annealing step at 575 °C. The peak position of the EBIC signal for sample 1789-425 indicates the electrical junction is significantly within the CIGS layer. The EBIC peak of sample 1789-575 is somewhat closer to the CIGS/CdS metallurgical junction.

Capacitance values of the three devices were measured as a function of frequency. The resulting C(f) data taken under zero bias conditions in the dark are shown in Fig. 6. Capacitance-voltage (C-V) data obtained under near-steady-state conditions with 100 seconds wait at each bias point is given in Fig. 7a in the form of $(A/C)^2$ vs. voltage curves.

The dispersion in the capacitance observed in Fig. 6 was the greatest for sample 1789-425, indicating the presence of a large density of extraneous states in the absorber. For this reason, the measurement frequency for C-V data was increased from 60 kHz to 500 kHz for this sample to minimizemthe apparent capacitance due to these extraneous states at lower frequencies. The zero bias capacitance value was the smallest for sample 1789-425, indicating the widest depletion width, despite the fact that the built-in potential was expected to be the smallest for this low-voltage device. The spatial variation of the hole density calculated from the slope of the Fig. 7a curves is shown in Fig. 7b for the three cells. The distance from the metallurgical junction is determined directly from the measured capacitance. According to Fig. 7b, the hole density in all films increases from less than $3x10^{15}$ cm^{-3} near the highly compensated surface region to about $3x10^{16}$ cm^{-3} at

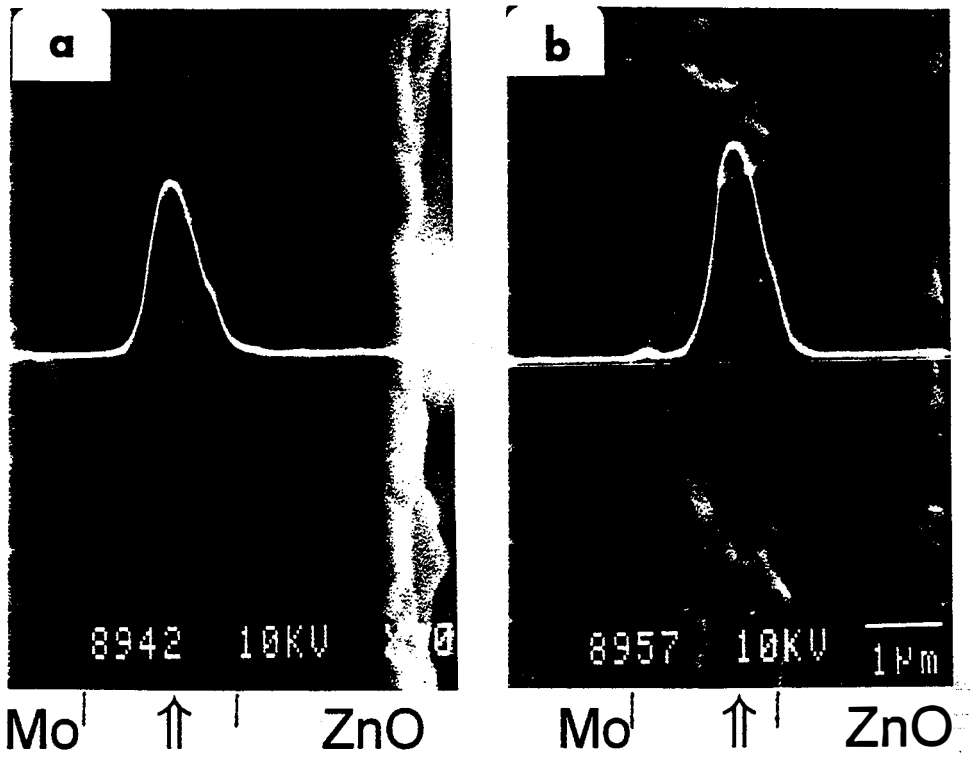

Fig. 5 Charge collection efficiency profiles (EBIC line scans) superimposed on scanning electron images of cross sections of samples (a) 1789-425 and (b) 1789-575. EBIC peak position is indicated with an arrow.

about 0.6-0.75 μm from the junction. The width of the low-density region has a magnitude comparable to the depth of the EBIC peak, and it appears to decrease from sample 1789-425 to 1789-575. This observation suggests the existence of a highly compensated thick surface layer in sample 1789-425 and a decrease in the thickness of this compensated layer as the active Ga content in the absorber layer was increased by the high-temperature annealing step.

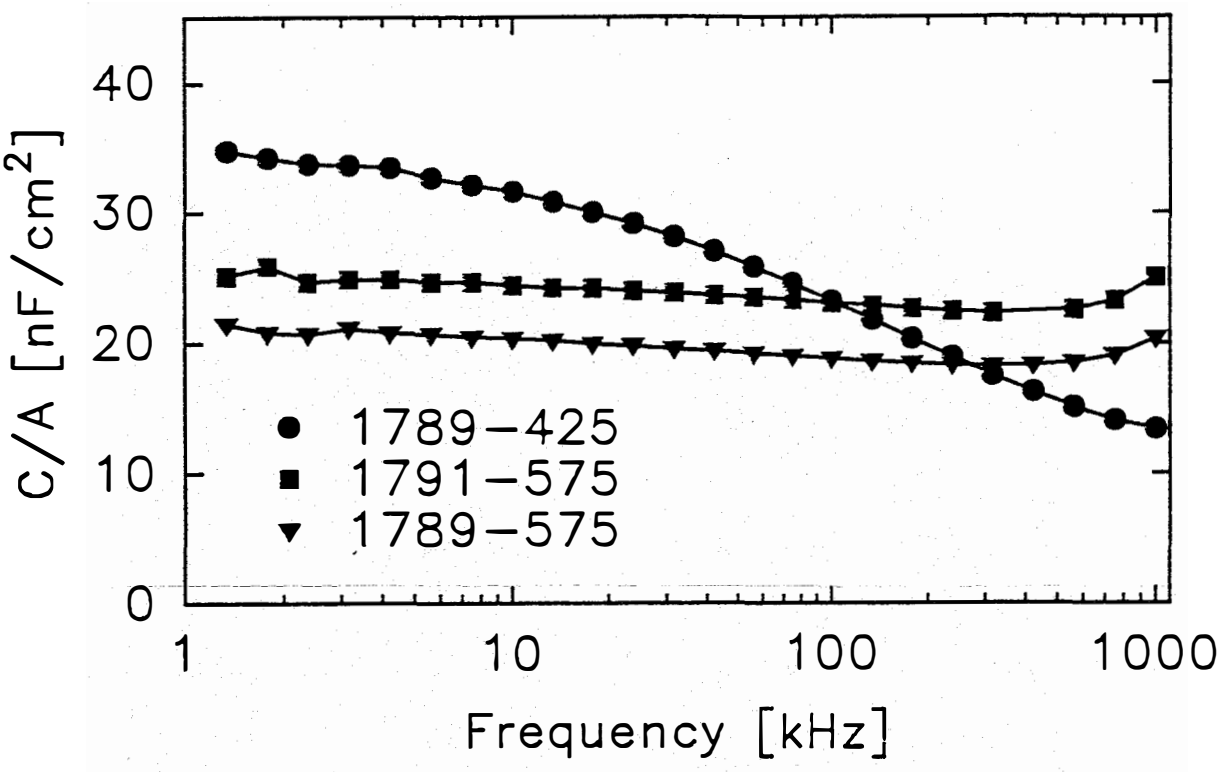

Fig. 6 Capacitance vs. frequency data for the cells of Fig. 3.

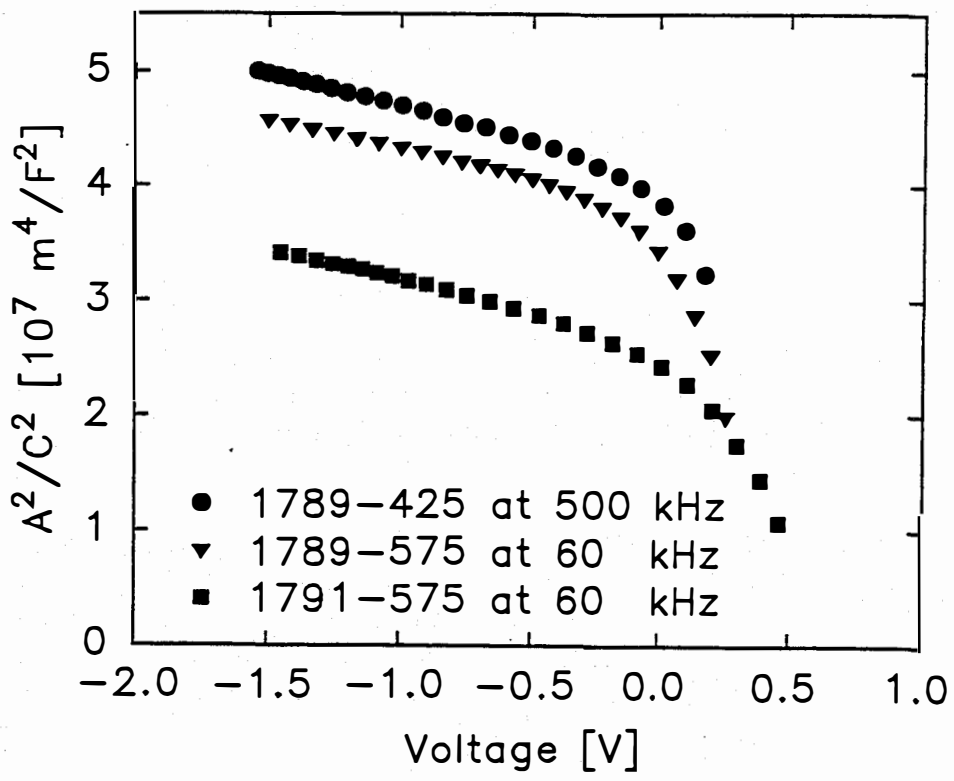

Fig. 7a $(A/C)^2$ vs. V data for the devices of Fig. 3.

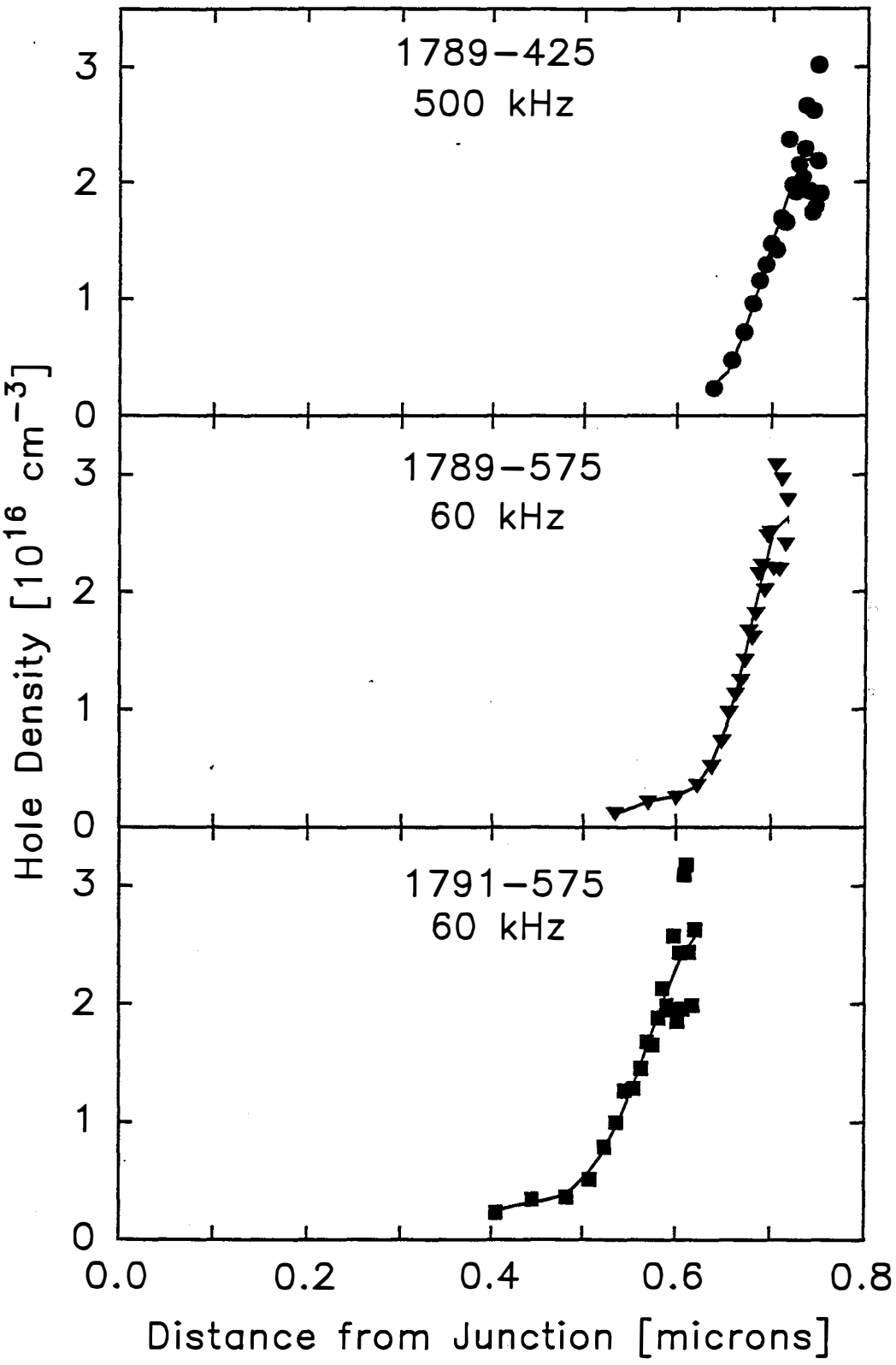

Fig. 7b Hole density distribution for the devices of Fig. 3.

B. Absorber Layer Characterization

Figure 8 shows the Auger depth profiles and the calculated Ga/(Ga+In) ratios of the CIGS films identified in Table I. As seen from these data, the compositions of samples 1789-425 and 1791-425, which were not subjected to the high-temperature annealing step after selenization, were highly graded suggesting segregation of In and Ga-rich phases. These films contained only small amounts of Ga near their surface, despite the fact that Ga was originally deposited on the surface of the precursor layers as described before. After the high-temperature annealing step, Ga concentration near the surface increased. However, the resulting absorbers were still graded in terms of their Ga distribution.

According to Fig. 8a, the Ga/(Ga+In) ratio for sample 1789-425 increases from about 0.1 at a region about 0.1 μm inside the film surface to 0.98 at a depth of 1.4 μm. The expected E_g value of the surface region with 10% Ga is 1.07 eV, which is in good agreement with the data of Table II. The Ga/(Ga+In) ratios near the surface regions of samples 1789-575 and 1791-575 are 0.31 and 0.53, respectively. These values are also in reasonably good agreement with the device measurement results that predicted the presence of CIGS phases with 28% and 50% Ga, respectively, in these two absorber layers.

Although the Ga/(Ga+In) ratios deduced from the calibrated Auger data of Fig. 8 agreed well with the results obtained from QE and V_{oc} measurements, the Cu/(In+Ga) stoichiometric ratios of Fig. 8 were unrealistically high for samples 1789-425 and 1791-425. These ratios were in the range of 1.2-2.2, especially near the surface regions of the two films, despite the fact that the stoichiometric ratios of all the films studied were fixed at 0.9 at the precursor stage before the selenization step. Also noticeable in the Auger data of Fig. 8a and Fig. 8c were the excessively high Se concentrations, again especially near the surface regions of the two films. Both of these abnormalities disappeared once the films were annealed at 575 °C. For the samples of Fig. 8b and Fig. 8d, the calculated Cu/(In+Ga) ratios approached 0.9 and Se concentration decreased to the 50%-53% range. We believe that the discrepancies observed between the Auger data of the two sets of films were due to the presence of binary phases in samples 1789-425 and 1791-425. The poor performance of the solar cell fabricated on sample 1789-425, its large capacitance dispersion, and the lack of photovoltaic activity for sample 1791-425, all support this argument. It is known that CGS formation requires higher temperatures than CIS formation. Therefore, the selenization temperature of 425 °C used in this study , although quite adequate for the growth of high-quality CIS layers, was not sufficient to form a CIS/CGS graded compound film. Therefore, films containing the CIS phase as well as the CGS ternary and Ga-Se and Cu-Se binaries were formed. It should be noted that the Auger data of Fig. 8 was calibrated using sensitivity factors of elements obtained from electron microprobe analysis of quaternary compound CIGS standards. Presence of binary phases in the analyzed layers are expected to affect the atomic concentration values plotted in the Auger profiles, because the sensitivity factors of elements in the binaries will be different than those used for the calibration of the reported experiment.

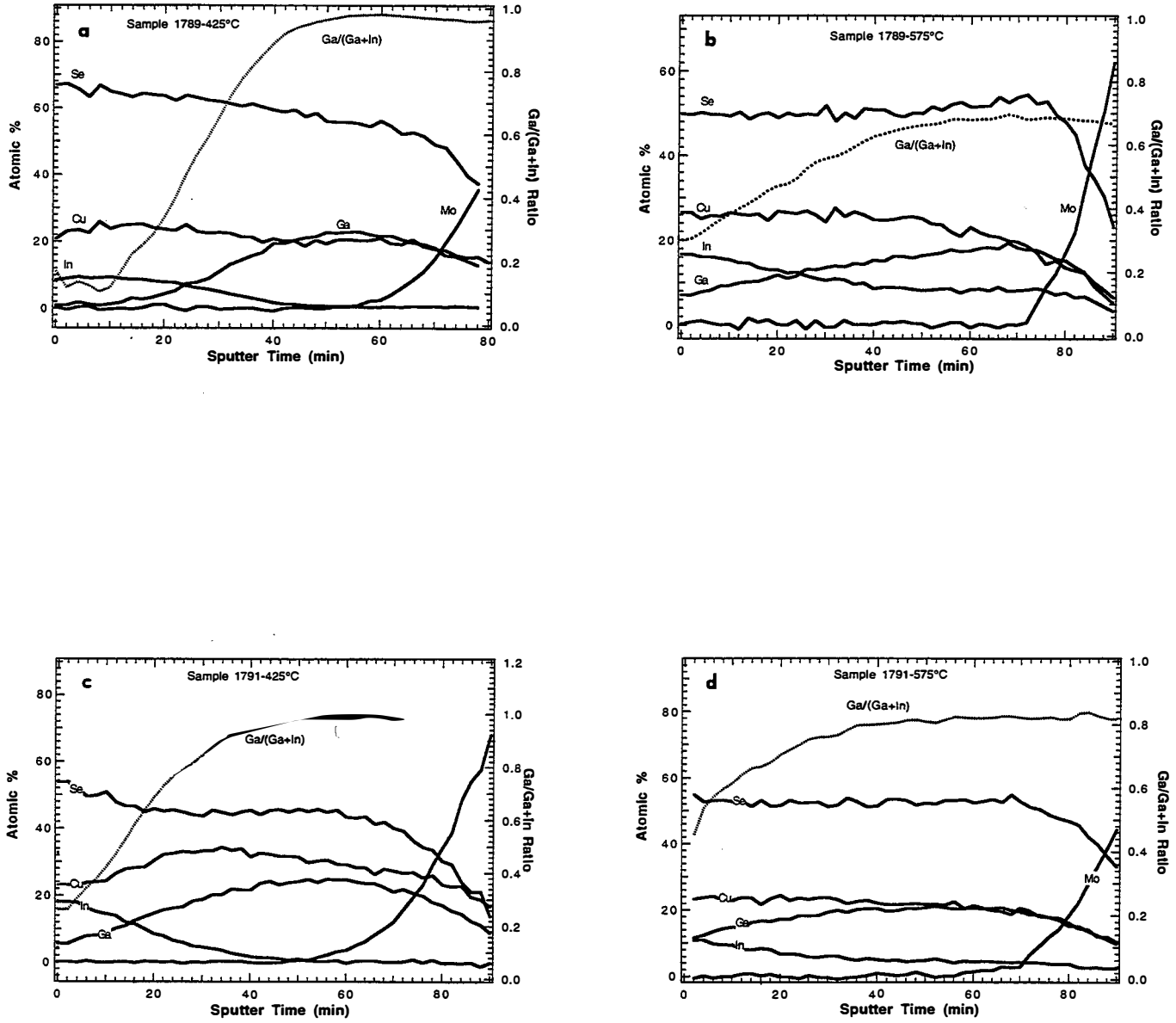

Fig. 8 Auger depth profiles of samples (a) 1789-425, (b) 1789-575,(c) 1791-425, and (d) 1791-575. The sputtering rate was 4-5 Å/sec.

Figure 9 shows the diffraction patterns obtained from two of the samples listed in Table I. Only the 2Θ values in the 44°-47° range have been scanned in this experiment to be able to resolve the (220) and (204) peaks of the tetragonal lattice. The expected positions of these peaks for CIS and CGS compounds were calculated and they are shown in Fig. 9. In sample 1789-425, the (220,204) peak belonging to tetragonal CIS is clearly resolved. The peak is shifted only slightly to higher angles suggesting inclusion of a small amount of Ga into the chalcopyrite absorber in agreement with the Auger and device measurements discussed before. Another observation from Fig. 9a is the total absence of the (220) and (204) doublet peaks belonging to tetragonal CGS. The low temperature employed for selenization of this sample was not expected to form tetragonal CGS. X-ray data from sample 1789-575 did not display the merged CIS peaks of (220,204) at 2Θ=44.35°. Instead, there is a broad peak shifted to higher angles indicating the formation of CIGS phase. The shape of the peak suggests that the film is not uniform and that there is a compositional gradient through the absorber confirming the Auger results.

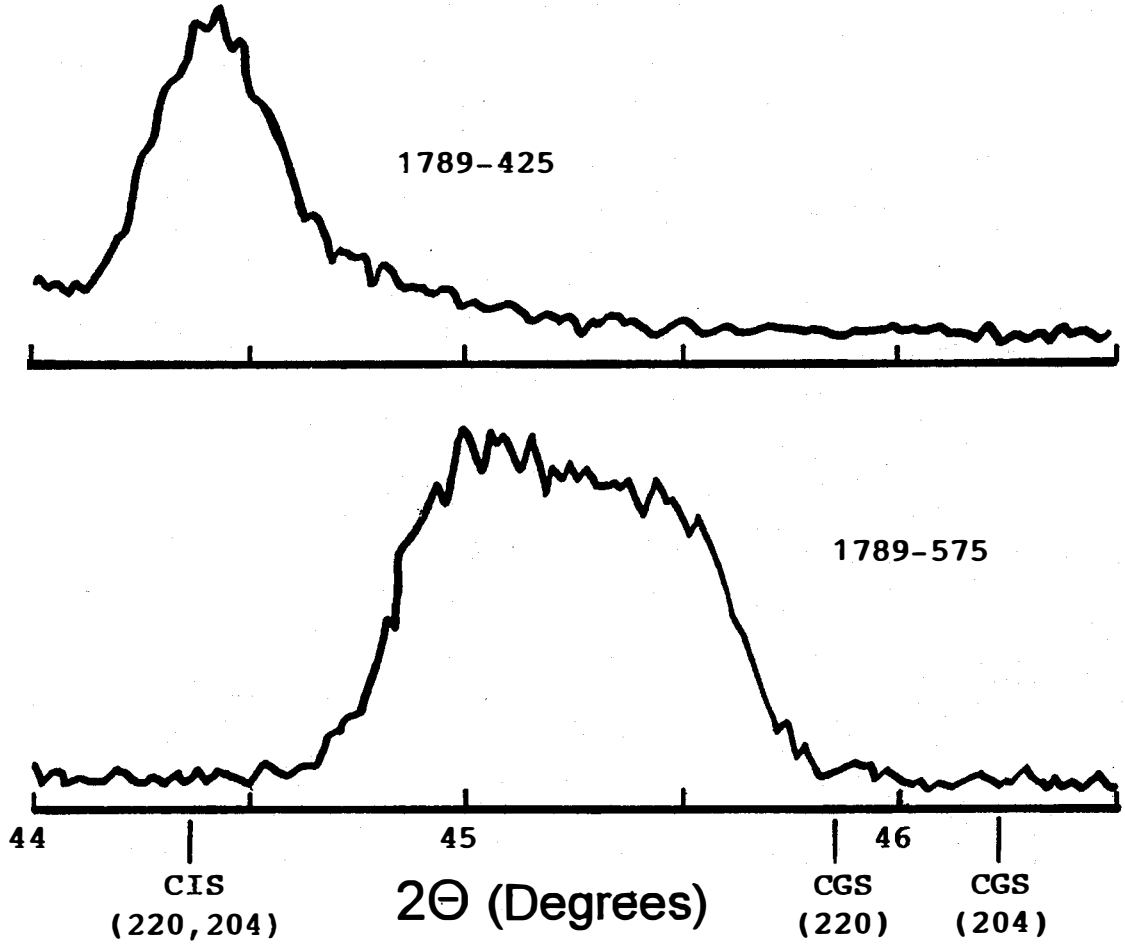

Fig. 9 XRD data taken from samples 1789-425 and 1789-575. The expected positions of the (220) and (204) peaks for CIS and CGS are indicated.

3.2.2 Films containing S

Experiments were carried out with the aim of including S into the CIS absorber layers and increasing their bandgaps. Sulfur inclusion involved a reaction step of the Cu-In precursors in Se and S containing environments. Concentrations of Se and S made available to the CIS film during the reaction step were varied to obtain layers with various S/(S+Se) ratios. A series of experiments were also carried out to determine the possibility of grading the S layer in the absorber.

Fig. 10 shows the two Auger depth profiles taken from two different $CuIn(S,Se)_2$ absorber layers. Sample 1810 was obtained using a precursor layer with Cu/(In+Ga) ratio of 0.88 and a Ga/(Ga+In) ratio of 0.15. Sample 1812, on the other hand, had a precursor with Cu/In ratio of 0.9 with no Ga. The amount of Se made available to Sample 1810 during the reaction step was approximately double the amount that was made available to Sample 1812. The following observations can be made from the data of Fig. 10.

The Ga concentration is graded through Sample 1810 and it peaks near the Mo interface as expected (Fig. 10a). Sulfur concentration follows the Ga concentration and it varies from about 17% near the surface to over 22% near the Mo interface. There is a small S peak near the surface region of Sample 1810. Se concentration in this sample is also variable and suggest a S/(S+Se) ratio varying from 0.37 near the surface to 0.63 in the back of the device. In Sample 1812 (Fig. 10b) the S distribution within the film is just the reverse of Sample 1810. In other words, S content decreases as one goes from the surface towards the back Mo contact. Also the peak S/(S+Se) ratio (about 0.73) for this sample is higher than that of Sample 1810. These differences are due to the different rates of reaction between S and Se and the Cu-In(Ga) precursor layer and they indicate the possibility of a degree of control over S gradation in the absorber layer.

Fig. 11a and 11b show the I-V characteristics of two small area (0.09 cm^2) cells fabricated on Samples 1810 and 1812. The open circuit voltage values of >0.55 V are in line with the fact that the absorber layers have wider bandgaps. The short circuit current density of Sample 1812 is extremely low (14.44 mA/cm^2) indicating very poor collection efficiency. This is understandable since the grading of S as shown in Fig. 10b is expected to form a barrier to the diffusion of generated electrons to the junction region. Any gradation of S near the junction should be sharp as in Fig. 10a so that this graded area is within the depletion region with high electric field. The device of Fig. 11a has an efficiency of about 10%.

Fig. 12 shows the I-V characteristics of three cells fabricated on three different types of absorbers. These absorbers were grown from the same metallic precursor film but during compound formation the amount of S and Se available to the films were varied. The relative amounts of Se/S species in the reactor are given in the caption of this figure. The increase in the open circuit voltage coupled with a decrease in the short circuit is in agreement with the variation of the S content in the three films.

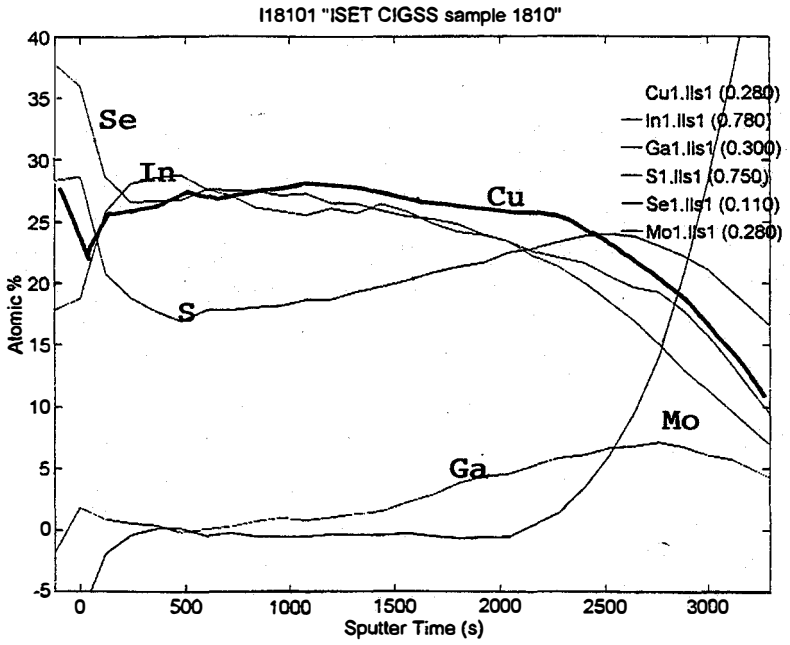

(a)

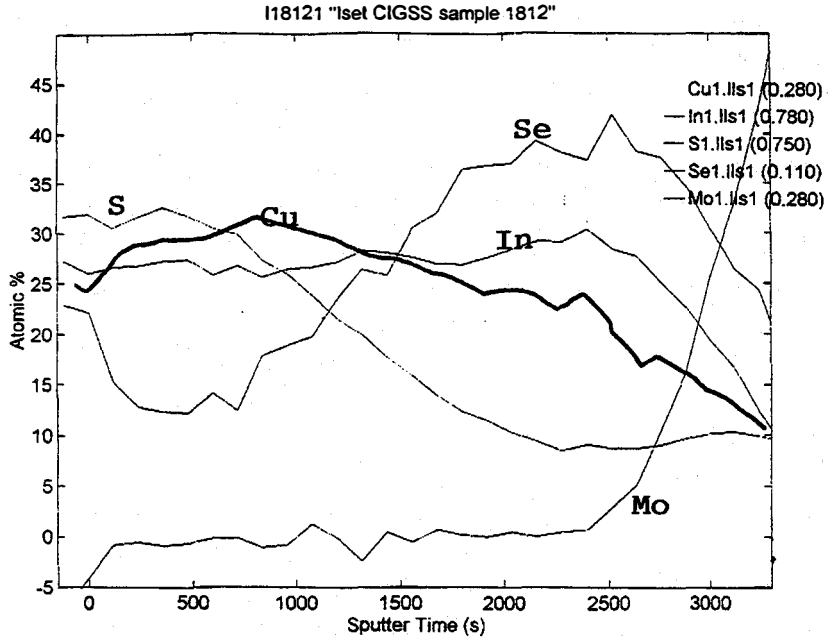

(b)

Fig. 10 Auger depth profiles of two $CuIn(S,Se)_2$ layers: a) Sample 1810, b) Sample 1812.

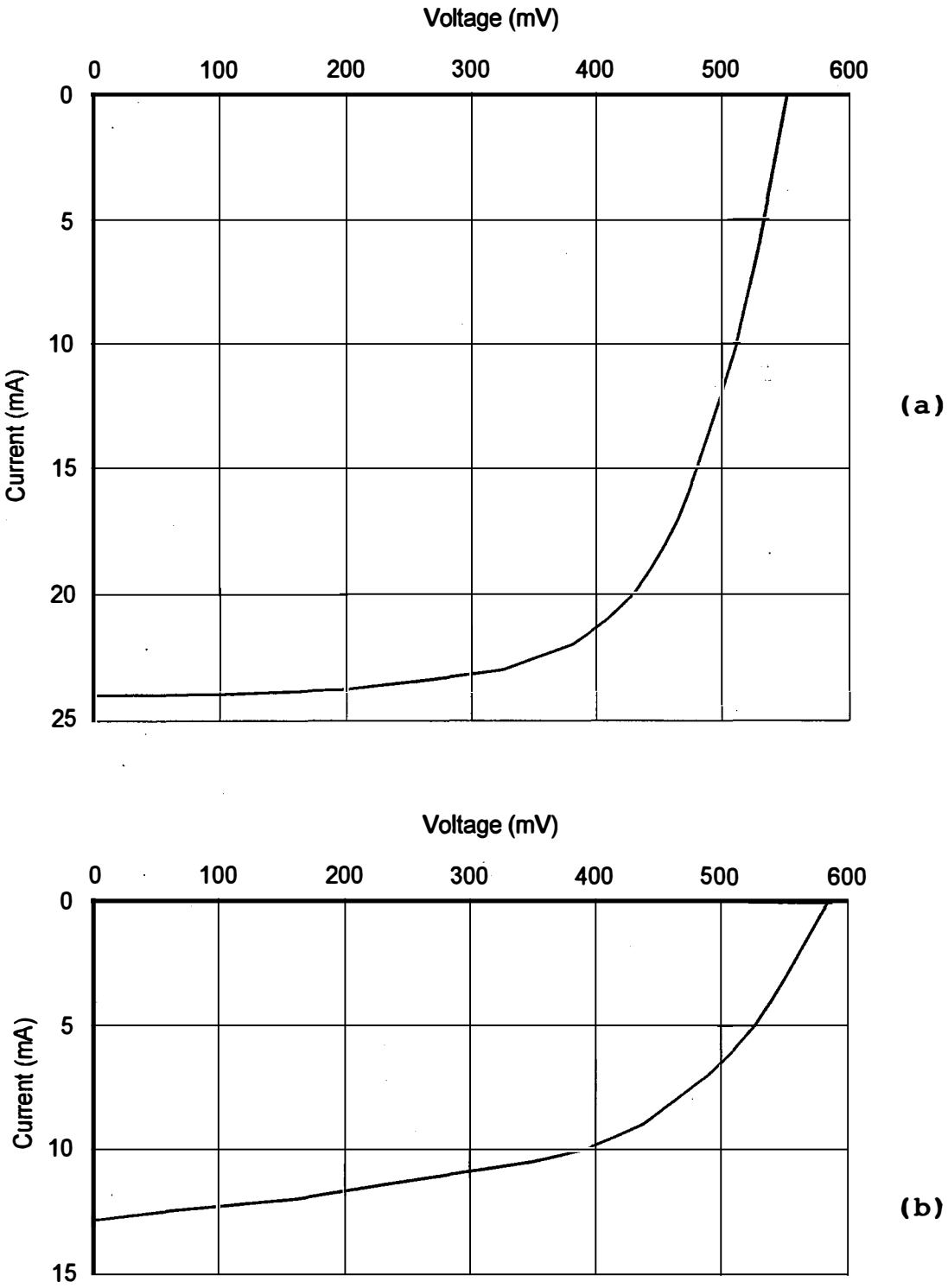

Fig. 11 Illuminated I-V characteristics of devices made on a) sample 1810, and b) sample 1812. The solar cell parameters of the device on Sample 1810 are V_{oc}=0.553 V, I_{sc}=2.41 mA, F=64.6% and eff.=9.57%. Active area efficiency is 10.3%.

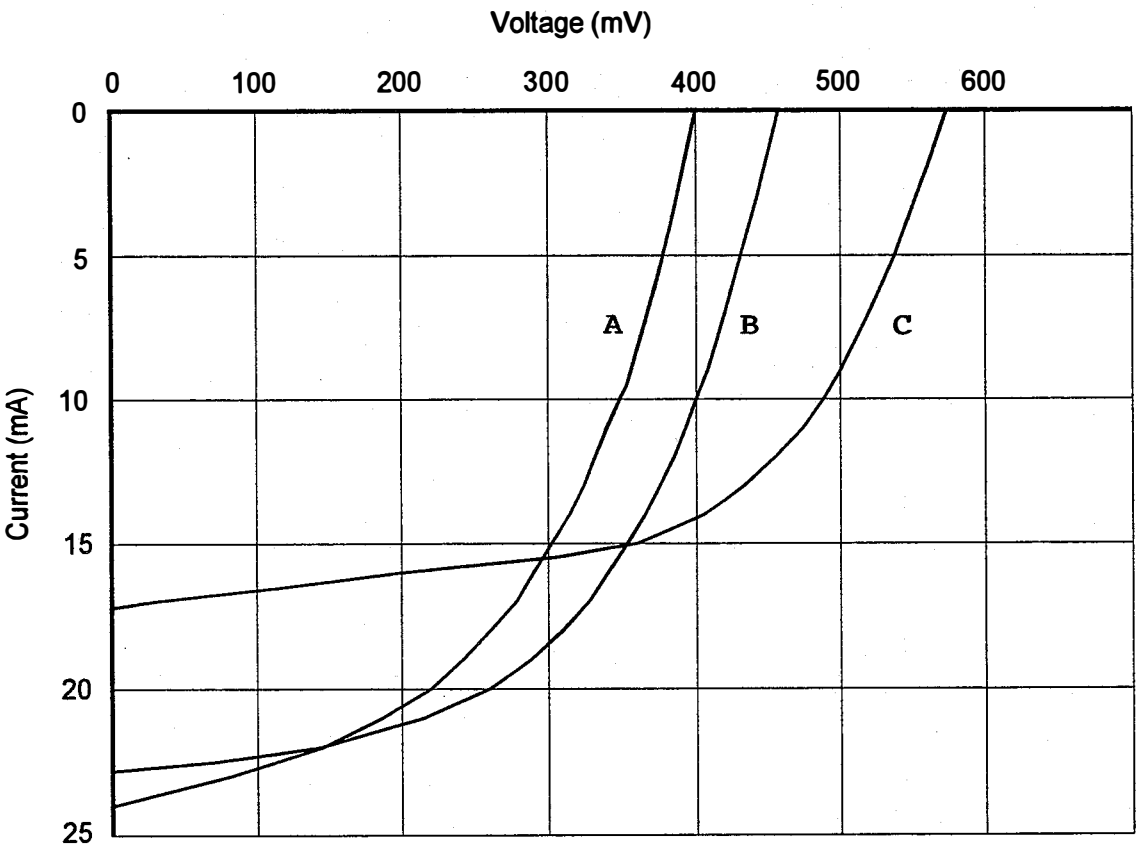

Fig. 12 Illuminated I-V characteristics of three $CuIn(S,Se)_2$ cells. Absorber of device A did not contain any S. Amount of S in device C was double that of B.

3.3 Novel CIS Deposition Technique

A primary concern in establishing CIS module manufacturing is the cost of capital equipment. In processes using vacuum techniques, this can be substantially high. Therefore, investigation into alternative methods of solar cell absorber processing exhibiting both low capital costs and low manufacturing costs are of great interest.

During Phase I of this project, efforts were concentrated on a novel non-vacuum CIS film deposition technique which has the potential of offering very low manufacturing costs. One of the most attractive features of this novel technique is that it uses established current-technology processes for device fabrication. A device structure used in many vacuum-based processes, namely glass/Mo/CIS/CdS/ZnO configuration, is also employed here. However, the formation of the CIS absorber layer is done by a non-vacuum process.

The device efficiencies have steadily improved during this Phase I program as a better understanding of the non-vacuum process is achieved. The I-V characteristics of the

highest efficiency cell produced to date is given in Fig. 13. The solar cell parameters of this device with 0.09 cm^2 area are; V_{oc} = 0.4728 V, J_{sc} = 38.46 mA/cm^2 and FF = 67.97%. The active area efficiency can be calculated to be 13.3 %. This is the highest efficiency CIS solar cell ever produced with a non-vacuum technique.

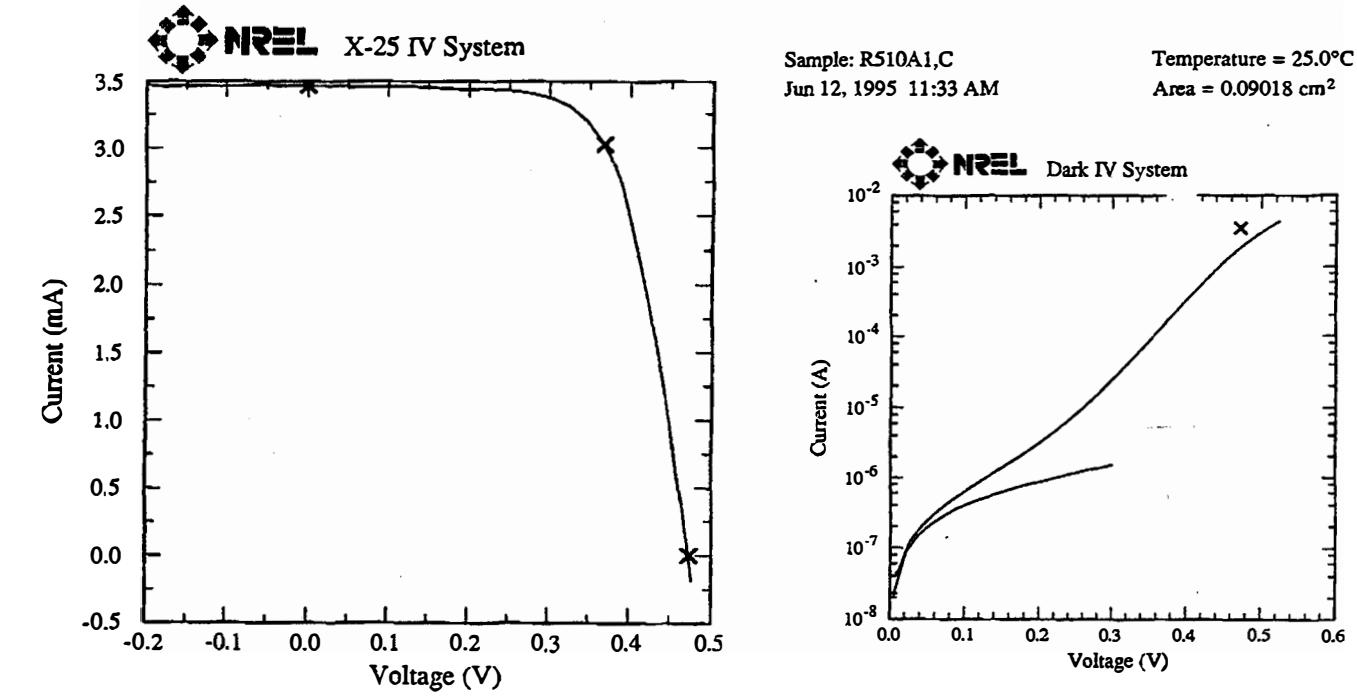

V_{oc} = 0.4728 V
I_{sc} = 3.468 mA
J_{sc} = 38.46 $mAcm^{-2}$
Fill Factor = 67.97 %

V_{max} = 0.3685 V
I_{max} = 3.025 mA
P_{max} = 1.115 mW
Efficiency = 12.4 %

V_{oc} = 0.4727 V
I_{sc} = 3.472 mA
Equiv Rs = 10.3 Ω

Rshunt = 155.5 kΩ
Rseries = 20.7 Ω

10 min @ P_{max},2 min cool,fast sweep
fan on during P_{max} soak to reduce heating

Fig. 13 Illuminated and dark I-V characteristics of a 0.09 cm^2 cell fabricated on a CIS layer grown by the non-vacuum technique.

Several solar cells with larger area were also fabricated during this period. One example of a 1 cm^2 device is shown in Fig. 14 along with its spectral response data. The response is flat with high transmission at short wavelengths. The long wavelength tail is in line with the pure CIS composition of the absorber. The AM1.5 total area conversion efficiency of this cell is 11.7 %.

Sample: R716F-A
Oct 4, 1995 9:10 AM
ASTM E 892-87 Global

Temperature = 25.0°C
Area = 1.008 cm^2
Irradiance: 1000.0 Wm^{-2}

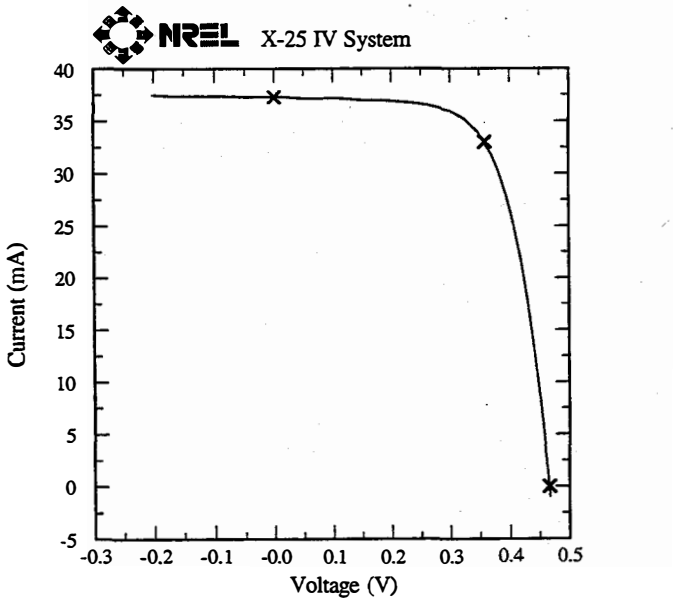

V_{oc} = 0.4666 V
I_{sc} = 37.01 mA
J_{sc} = 36.71 $mAcm^{-2}$
Fill Factor = 68.24 %

V_{max} = 0.3595 V
I_{max} = 32.78 mA
P_{max} = 11.78 mW
Efficiency = 11.7 %

10 min soak @ P_{max},2 min cool

Sample: R716F-A
Oct 6, 1995 9:41 AM

Temperature = 25.0°C
Device Area = 1.008 cm^2

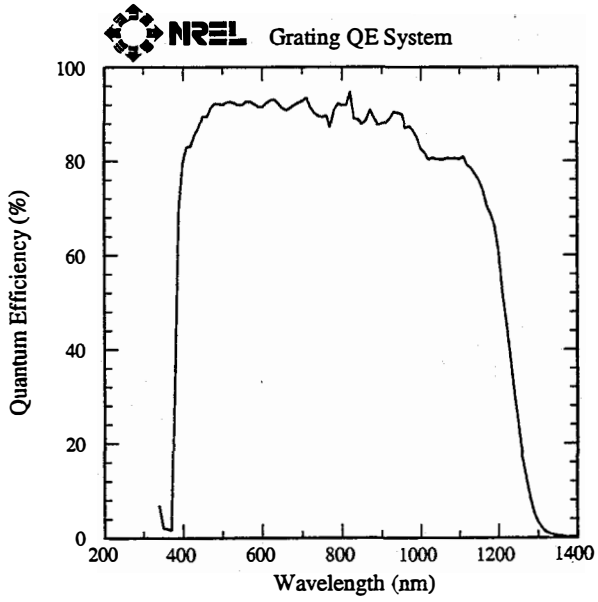

zero voltage bias
Light Bias = 5.00 mA

Compare with Filter QE measurement

Fig. 14 Characteristics of a 1 cm^2 CIS solar cell fabricated on non-vacuum absorber.

Characterization of a group of high efficiency devices fabricated on CIS absorbers grown by the non-vacuum technique was carried out at CSU by Prof. J. Sites' group. The cell output parameters and diode characteristics of three such devices are given in Tables III and IV, respectively. The devices are quite similar with illuminated series resistance values

in the 0.02-0.03 ohm-cm^2 range. The diode factors are 1.6-1.75. Comparing these parameters with those of cells fabricated on CIS films grown by our vacuum based selenization technique we find that the A factors are somewhat higher than what we obtain in the high efficiency vacuum based devices. The hole densities calculated from the C-V data of the cells are shown in Fig. 15. The values range from mid-10^{15} to just above 10^{16} /cm^3. These results also compare well with the data previously taken from vacuum based solar cells.

Cell R510A1	Area [cm^2]	η	FF	V_{oc} [mV]	J_{sc} [mA/cm^2]
A	0.09059	11.9	.670	465	38.14
B	0.09117	12.5	.700	470	38.06
C	0.09018	11.8	.665	460	38.46

Table III Cell output parameters.

Cell R510A1	A_{light}	R_{light} [Ω-cm^2]	r_{light} [Ω-cm^2]	A_{dark}	R_{dark} [Ω-cm^2]	r_{dark} [Ω-cm^2]
A	1.65	0.3	750	1.55	0.03	4150
B	1.60	0.3	1300	1.55	0.05	3400
C	1.75	0.2	600	1.55	0.06	5500

Table IV Diode characteristics.

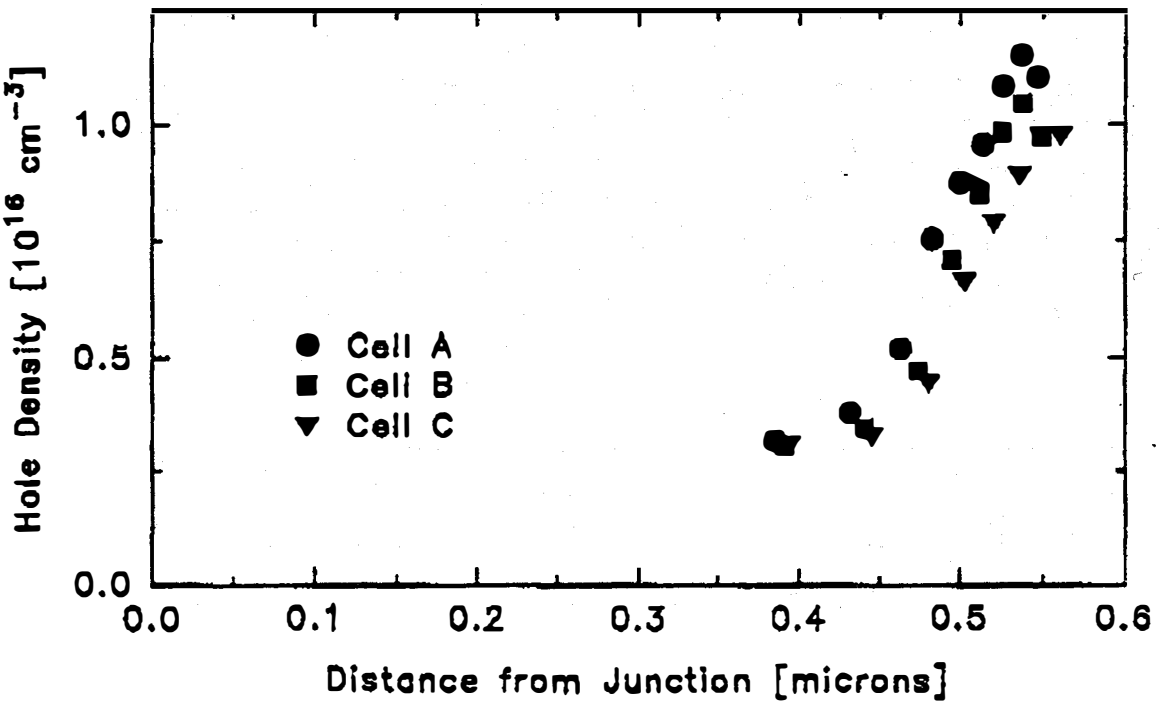

Fig. 15 Hole density values calculated for the CIS layers grown by the non-vacuum technique.

The spectral response data taken from cell A of Table III is shown in Fig. 16. Current losses due to various mechanisms are also indicated in this figure. Reflection loss is the largest contributor to the less-than-ideal current density value. It should be noted that none of the devices reported in this Final Technical Report had A/R coatings deposited on them.

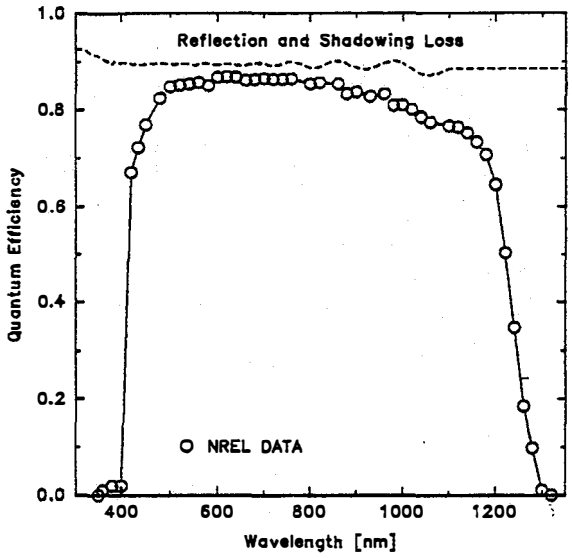

NREL Data normalized to reported J_{sc} of 38.14 mA/cm^2

Loss Currents in mA/cm^2

Window Loss	2.0
Deep penetration Loss	3.3
Reflection Loss	4.2
Probe Shadow Loss (estimated)	1.0

Fig. 16 Quantum efficiency data for cell A of Table III.

In addition to discrete cell fabrication, work was also done to fabricate integrated modules on CIS layers grown by the novel non-vacuum technique. The module integration approach was the same as the technique utilized on vacuum based devices [1]. The Mo scribing was done by laser. The two scribes following the CIS and ZnO depositions were done mechanically. The I-V characteristics and the spectral response of a 25 cm^2 sub-module is given in Fig. 17. Comparing the spectral response data of this submodule with that of the single cell of Fig. 16 one can see that the long wavelength response suffers in the module structure. This is due to the fact that the module structure uses 5 ohms/square ZnO layer as compared with the 15-20 ohms/square material used in discrete cell structures. Thicker ZnO layers absorb more in infrared due to free carrier absorption and this reflects into the long wavelength response of the device.

Sample: R627
May 16, 1995 2:27 PM
ASTM E 892-87 Global

Temperature = 25.0°C
Area = 24.71 cm^2
Irradiance: 1000.0 Wm^{-2}

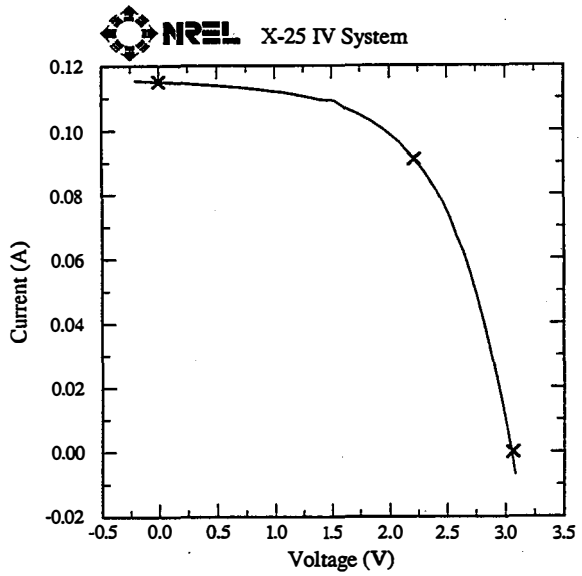

V_{oc} = 3.063 V
I_{sc} = 0.1150 A
J_{sc} = 4.655 $mAcm^{-2}$
Fill Factor = 57.27 %

V_{max} = 2.217 V
I_{max} = 0.09104 A
P_{max} = 201.8 mW
Efficiency = 8.17 %

after 5 min at P_{max}, and cool down

Sample: R627
May 15, 1995 2:32 PM

Temperature = 25.0°C
Device Area = 24.71 cm^2

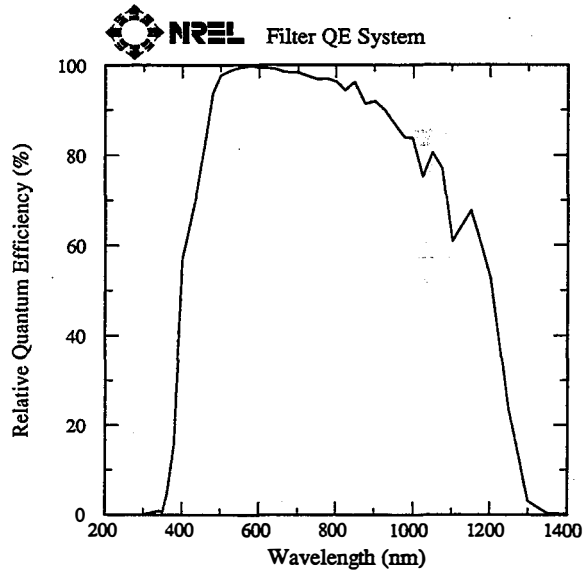

Light Bias = 13.200 mA
Bias Voltage = 0.00 V

J_{sc} = 41.32 mA/cm^2 for ASTM E 892 Global (1000 W/m^2) Spectrum

Fig. 17 A 25 cm^2 submodule fabricated on a CIS layer grown by the non-vacuum technique.

4.0 CONCLUSIONS AND FUTURE WORK

During the last 12 months of this Phase I development program we concentrated on three main topics:

i) Interactions between the Mo/glass substrates and the CIS absorber layers as well as the selenization atmosphere were studied. Na diffusion through the Mo layer was found to be responsible for excessive reaction between the substrates and absorbers in certain samples. This interaction was found to affect the stoichiometric uniformity of thin CIS layers grown on such Mo/glass substrates. Placement of a diffusion barrier on the glass substrate or use of a Mo layer that acts as an effective barrier to Na diffusion are two approaches that can avoid excessive reactions at the CIS/Mo interface which were shown to negatively impact the solar cell efficiency.

ii) Ga and/or S were successfully added to the CIS absorber layers for bandgap tailoring. Devices with high open circuit voltages and 10-12% efficiency have been demonstrated on these higher bandgap absorbers. Ga addition and its activation in the film required a high temperature annealing step which followed the selenization of the Cu-In-Ga metallic precursors. This annealing step caused the diffusion of Ga towards the surface of the absorber from the absorber/Mo interface where it normally is located after the selenization step. Sulfur addition into the absorbers required the use of reaction atmospheres containing both S and Se. Depending upon the choice of S/Se source and the reaction temperatures, various S profiles could be obtained in these absorbers.

iii) A novel, non-vacuum technique for the growth of CIS absorbers was successfully developed and both high efficiency cells and submodules were demonstrated for the first time on such absorbers. The highest efficiency obtained for single cells to date is 12.4% (13.3% active area) for small area devices. A submodule efficiency of above 8% has also been obtained for a 25 cm^2 device.

Work during the second year of this effort will concentrate on building a pilot processing facility that can produce 5"x12" size submodules using the non-vacuum CIS film growth technique. Work will also be carried out to include S and Ga into these absorbers. Results obtained on the samples grown by the vacuum technique will be very helpful in this task. The substrate influence on CIS layer growth (Na-diffusion) is expected to be a factor to be taken into account even in the non-vacuum growth technique. Therefore, we will concentrate on the use of a Na barrier on the glass surface for this work to be able to isolate the substrate effect from other parameters that may affect growth . Na addition in the CIS film will then be achived during the growth process since it is known that presence of Na in the absorber is beneficial to the electronic and possibly the structural properties of this layer.

5.0 ACKNOWLEDGMENTS

The authors are grateful to R. Matson, A. Swartzlander-Franz, A. Nelson, A. Mason, H. Field and K. Emery of NREL for characterization and measurements of films and devices, and to H. Ullal, R. Noufi and K. Zweibel for extensive technical discussions. Authors gratefully acknowledge the contributions of Dr. Robert Birkmire of IEC, Dr. J. Sites, J. Sharp and J. Granata of CSU to the reported work .

6.0 LIST OF PUBLICATIONS

During the last 12 month period the following publications were published on the subject of thin film solar cells:

B.M. Başol, V.K. Kapur, C.R. Leidholm, A. Halani and A. Minnick , "Studies on Thin Film CIGS Solar Cells and Modules", 13th NREL PV Program Rev., AIP Conf. Ser. 353, 1995, p. 26.

J.R. Tuttle et al., "Characterization and Modeling of CIGS based PV Devices: A Laboratory and Industrial Perspective", Progress in PV, 3, 89 (1995).

B.M. Başol, V.K. Kapur, A. Halani, C.R. Leidholm, J. Sharp, J. Sites, A. Swartzlander, R. Matson and H. Ullal, "CIGS Thin Films and Solar Cells Prepared by Selenization of Metallic Precursors", J. Vac. Sci. Technol. A., (in press).

B.M. Başol, V.K. Kapur, C.R. Leidholm, A. Halani and K. Gledhill, "Flexible and Light Weight CIS Solar Cells on Polyimide Substrates", Sol. Energy Matl. Sol. Cells, (in press).

7.0 REFERENCES

1. B.M. Başol, V.K. Kapur, A. Halani and C. Leidholm, "Novel two-stage selenization methods for fabrication of thin film CIS cells and submodules" , Final Subcontract Report, March 1, 1993-March 31, 1995. Subcontract No. YI-2-12069-1.
2. R. Brown in "Handbook of thin film technology" eds.L. Maissel and R. Glang, McGraw Hill, 1970, p. 6-8.
3. M.A. Contreras, J. Tuttle, A. Gabor, A. Tennant, K. Ramanathan, S. Asher, A. Franz, J. Keane, L. Wang, J. Scofield and R. Noufi, Proc. IEEE 1st World Conf. on PV Energy Conversion, Hawaii, 1994, p. 68.
4. K. Kushiya, A. Shimizu, K. Saito, A. Yamada and M. Konagai, Proc. IEEE 1st World Conf. on PV Energy Conversion, Hawaii, 1994, p. 87.
5. D.S. Albin, J.R. Tuttle, M. Contreras, A.M. Gabor, A. Mason, R. Noufi and P. Singh, Solar Energy Materials and Solar Cells (in press).
6. M. Marudachalam, R. Birkmire, J.M. Schultz, and T. Yokimcus, Proc. IEEE 1st World Conf. on PV Energy Conversion, Hawaii, 1994, p. 234.
7. B.M. Başol, V.K. Kapur, C. Leidholm, A. Halani and A. Minnick, 13th NREL PV Program Review Meeting, Lakewood, Colorado, May 16-19, 1995, AIP Conf. Proceeding (in press).

REPORT DOCUMENTATION PAGE

Form Approved
OMB NO. 0704-0188

1. AGENCY USE ONLY (Leave blank)	2. REPORT DATE	3. REPORT TYPE AND DATES COVERED
	June 1996	Annual Technical Progress Report, 1 April 1995 - 31 March 1996

4. TITLE AND SUBTITLE

Application of CIS to High-Efficiency PV Module Fabrication

5. FUNDING NUMBERS

C: ZAF-5-14142-07
TA: PV631101

6. AUTHOR(S)

B. Başol, V. Kapur, C. Leidholm, and A. Halani

7. PERFORMING ORGANIZATION NAME(S) AND ADDRESS(ES)

International Solar Electric Technology
8635 Aviation Blvd.
Inglewood, California 90301

8. PERFORMING ORGANIZATION REPORT NUMBER

9. SPONSORING/MONITORING AGENCY NAME(S) AND ADDRESS(ES)

National Renewable Energy Laboratory
1617 Cole Blvd.
Golden, CO 80401-3393

10. SPONSORING/MONITORING AGENCY REPORT NUMBER

TP-413-21355

DE96007913

11. SUPPLEMENTARY NOTES

NREL Technical Monitor: H.S. Ullal

12a. DISTRIBUTION/AVAILABILITY STATEMENT

12b. DISTRIBUTION CODE

UC-1260

13. ABSTRACT *(Maximum 200 words)*

We investigated the interactions between the soda-lime glass substrate, the Mo contact film and the CIS absorber layer. Excessive Na diffusion through the Mo layer was found to be the reason for excessive interaction between the substrate and the CIS layers obtained by the H_2Se selenization technique. This chemical interaction influenced the stoichiometric uniformity of the absorbers. Addition of Ga into the CIS layers by the two-stage selenization technique yielded graded absorber structures with higher Ga content near the Mo/absorber interface. Gallium was later diffused through the absorber film by a high-temperature annealing step, and large bandgap alloys were obtained. Solar cells with active-area efficiencies of close to 12% were fabricated on these CIGS layers. Sulfur addition experiments were also carried out during this period. By controlling the Se and S availability to the precursors during the reaction step of the process, various S profiles were obtained in high-bandgap absorber layers. The highest-efficiency cell made on S-containing absorbers was about 10% efficient. A low-cost, non-vacuum technique was successfully developed for CIS film growth. Layers prepared using this novel approach were used for solar-cell and submodule fabrication. Solar cells with active-area efficiencies around 13% were demonstrated; submodules with efficiencies above 8% were also fabricated. These results represent the best PV devices ever produced on CIS layers obtained by a non-vacuum technique.

14. SUBJECT TERMS

photovoltaics ; CIS ; module fabrication ; non-vacuum technique

15. NUMBER OF PAGES
37

16. PRICE CODE

17. SECURITY CLASSIFICATION OF REPORT	18. SECURITY CLASSIFICATION OF THIS PAGE	19. SECURITY CLASSIFICATION OF ABSTRACT	20. LIMITATION OF ABSTRACT
Unclassified	Unclassified	Unclassified	UL